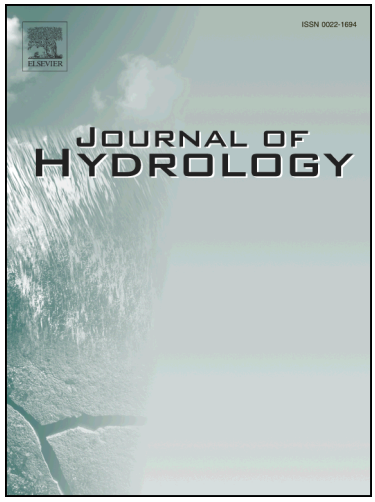

Research papers

Using a 2D shallow water model to assess Large-scale Particle Image Velocimetry (LSPIV) and Structure from Motion (SfM) techniques in a street-scale urban drainage physical model

J. Naves, J. Anta, J. Puertas, M. Regueiro-Picallo, J. Suárez

PII: S0022-1694(19)30439-1
DOI: https://doi.org/10.1016/j.jhydrol.2019.05.003
Reference: HYDROL 23736

To appear in: *Journal of Hydrology*

Received Date: 2 January 2019
Revised Date: 4 April 2019
Accepted Date: 1 May 2019

Please cite this article as: Naves, J., Anta, J., Puertas, J., Regueiro-Picallo, M., Suárez, J., Using a 2D shallow water model to assess Large-scale Particle Image Velocimetry (LSPIV) and Structure from Motion (SfM) techniques in a street-scale urban drainage physical model, *Journal of Hydrology* (2019), doi: https://doi.org/10.1016/j.jhydrol.2019.05.003

Using a 2D shallow water model to assess Large-scale Particle Image Velocimetry (LSPIV) and Structure from Motion (SfM) techniques in a street-scale urban drainage physical model

Naves[1,*], J., Anta[1], J., Puertas[1], J., Regueiro-Picallo[1], M. and Suárez[1], J.

[1]. Universidade da Coruña, Water and Environmental Engineering Research Team (GEAMA), Civil Engineering School, Elviña, 15071 A Coruña, Spain

*. Corresponding author

e-mail address: juan.naves@udc.es (Juan Naves)

ABSTRACT

Physically-based numerical modelling of surface processes in urban drainage, such as pollutant wash-off or the assessment of flood risks, requires appropriate calibration and terrain elevation data to properly simulate the overland flows and thus to achieve useful results. Accordingly, this study aims to obtain an accurate representation of the runoff generated by three different rain intensities, 30, 50 and 80 mm/h, in a full-scale urban drainage physical model of 36 m^2. The study focuses firstly on applying the Structure from Motion (SfM) photogrammetric technique to carry out a high-resolution and accurate topographic survey. This topography was implemented in a 2D shallow water model and the results were compared with those obtained using conventional manually data point measured topography. Negligible differences were found when comparing the two models with measured discharges at the physical model gully pots. However, significant differences were obtained in the velocity distributions, especially in the shallowest flow areas where drainage channels of a few millimeters' depth appeared in the high resolution topographic survey. Results from the numerical model were compared with overland flow velocities, determined by applying a modified Large Scale Particle Image Velocimetry (LSPIV) methodology using fluorescent particles. With the SfM topography, the 2D model was able to obtain a better representation of the experimental data, since small scale irregularities of the pavement surface could be represented in the model domain. At the same time, LSPIV was presented as a very suitable tool for the accurate measurement of runoff velocities in urban drainage models, avoiding the interference of raindrop features in the recorded images and with overland water depths in the order of few millimeters.

KEYWORDS:

LSPIV: large scale particle image velocimetry

SFM: structure from motion

Urban runoff

Physical model

2D shallow water model

Urban drainage

1. INTRODUCTION

Physically-based urban drainage models are commonly used tools to predict urban floods or sewer system discharges (e.g. Chen et al. 2009, Leandro et al. 2009, Neal et al. 2009). The calibration of these models is often performed with data taken from the sewer network, principally flow discharges and water depths (e.g. Seyoum et al., 2012, Hong et al., 2016a). Nevertheless, there are significant processes related to overland flows, such as flood risk management (e.g. Martínez-Gomariz et al. 2016, 2017, 2018) and the determination of the mobilization of the deposited pollutants over the street surface (e.g. Deletic et al., 1997, Egodawatta et al., 2007, Muthusamy et al., 2018). In these applications a good characterization of the surface flow is essential to achieve useful and accurate results. However, the difficulty in obtaining data on velocity fields and depths in overland flows makes the calibration of models a difficult task (Leitão et al. 2018).

In addition to the need for appropriate hydraulic calibration data, an accurate topography of the catchment is also required to simulate the urban runoff properly (Almeida et al. 2016). Using inaccurate elevation maps for modelling the surface flow by means of a 2D shallow water model can lead to erroneous results regarding the determination of the extent of floods or flood risks (Hunter et al. 2008). Besides flood analysis, in the study of sediment wash-off during non-extreme rain events, the influence of the topography is also relevant in the model outputs. Thus, sediment

transport capacity is influenced by the small overland flows depths, which may also hinder rainfall erosion capacity due to the impact of raindrops (Tomanovic and Maksimovic, 1996). These both factors increase the sensitivity of the model's results to the topography, and at the same time make it more difficult to measure undisturbed water depths and overland flow velocities in order to calibrate the model. Furthermore, in studies of this type, such as the one developed by Hong et al. (2016a, b), an accurate spatial and temporal representation of the runoff is key to reducing the propagation of hydraulic uncertainties to the sediment transport equations, since the hydraulic variables are used as an input for the flow-driven erosion, the transport, and the eventual deposition of sediments (Hairsine and Rose, 1992a, b).

The sensitivity to the model topography is greater in the case of small catchments or laboratory physical models, where a reduced area is considered (e.g. Wijesiri et al., 2015, Naves et al., 2017, Muthusamy et al., 2018). In typical urban flooding studies with 2D shallow water models, the topography is usually derived from airborne LiDAR with a resolution of about 0.25 m to 1.00 m, with root mean square errors (RMSE) for elevations of about 5 - 15 cm (Hunter et al., 2008, Neal et al., 2009, Fraga et al. 2016). This spatial resolution may be insufficiently accurate for a physically based approach of sediment wash-off, in which the elements of the digital terrain models are in the order of a few centimeters or even millimeters. In such cases, a terrestrial laser topography or on-vehicle LiDAR (Hong et al. 2016a), combined with conventional topographic techniques, can provide high-resolution and precise elevation data, but this implies a significant economic cost.

In this regard, visualization techniques are presented as a possible low-cost alternative to traditional methodologies for obtaining high-resolution elevation grid data. The photogrammetric technique Structure from Motion (SfM), which is based on stereoscopic principles, allows the reconstruction of a 3D object by means of overlapping images. Traditional photogrammetric methods require the location and positioning of cameras, or the location of ground control points to create a 3D object

reconstruction. In contrast, SfM method solves the geometry and the position and orientation automatically, using a highly redundant bundle adjustment based on matching features in multiple overlapping and offsetting of images (Westoby *et al*. 2012). This greatly simplifies the methodology and makes it more affordable for non-expert users. Although this technique is being used widely in river bathymetric applications (see for instance the review in Detert et al. 2017), in the field of urban drainage the applications are still quite limited. We can cite here only some previous studies developed by the current authors to determine the topography of sewer sediment deposits at the laboratory scale (Regueiro-Picallo *et al*. 2018).

As noted above, a non-adequate topography can lead to the erroneous modelling of spatial and temporal surface flow distributions. But even with a very accurate digital terrain model, measured data such as discharges, water depth, and flow velocities are required in order to calibrate and validate models, and thus to obtain useful results (Hunter et al., 2008). The measurement of shallow flows generated in urban catchment surfaces do not allow for the use of traditional methods, since these techniques interfere with the observed flow. Likewise, flow sensors used in pipe flows are often quite large and affect to the determination of the hydraulic variables.

The non-intrusive Particle Image Velocimetry (PIV) techniques are considered a suitable solution, and are commonly used in laboratory and field studies to obtain velocity-field datasets (Adrian, 1991, Raffel et al., 2007). PIV determines the displacement of particles seeded in the flow using cross-correlation methods on two image frames with a known time step between them. Large-scale PIV (LSPIV), proposed by Fujita et al. (1998), uses particles or other traces on the surface of the water flow, which are supposed to follow the same velocity. This variant uses the surface of the flow as the measurable plane, so it is easier to apply to field and realistic studies since the area under study can be much larger and expensive equipment such as complex lasers or cameras are not needed. Therefore, LSPIV methods are generally applied to measure surface velocities rather than depth averaged velocities,

and errors in the determination of depth-averaged flow velocities may become more significant at higher flow depths.

LSPIV is commonly used in river surveys (Le Coz et al., 2010, Muste et al., 2011) to determine river discharges. In order to transform surface velocities into depth-averaged velocities, and subsequently the discharge, a velocity index of 0.85 is typically used, although this correction factor is not appropriate for all measurement situations and depends on flow nature, flow regime (steady or un-steady) and bed roughness (Muste et al., 2011). Furthermore, the LSPIV technique has also been used for measuring shallow water flows in laboratory studies (Weitbrecht et al., 2002). For example, Kantoush et al. (2008) and Novak et al. (2017) apply LSPIV to investigate the flow field using artificial particles in a rectangular shallow reservoir and in an open-channel flow, respectively. In the case of Arques et al. (2018), by synchronizing four cameras, it was possible to resolve a large measurement area of 4.8 m x 1.22 m with high resolution LSPIV.

In the field of urban drainage, some studies using LSPIV in high water level conditions during flood events have recently been published. Guillén et al. (2017) presented a new approach to the study of the vulnerability of vehicles and people, where the LSPIV method is used to obtain superficial velocities from a domestic video. Martins et al. (2018) performed an extensive comparison between experimentally measured and numerically modelled flows for different manhole grate configurations. For this purpose, a detailed characterization of the velocity fields around these elements was performed by means of LSPIV. Leitão et al. (2018) presented the use of surveillance camera footage as a low-maintenance and easy-to-install alternative to measure surface flow by means of this image velocimetry. However, in the case of very shallow depths in non-extreme rain events, only a very preliminary measurement of the velocity of a small area using artificial tracers was found (Branisavljević and Prodanović, 2006). Because of its solid performance in the different studies cited above, LSPIV can be considered as a suitable technique for obtaining velocity-field

datasets with low water levels in urban areas. Nevertheless, due to small water depths here, commonly lower than 1 cm, and the presence of raindrops, which impact on the water surface and interfere in the surface flow and the recorded images, the accurate measurement of the velocities is a highly challenging task.

This study aims to achieve an accurate representation of the overland runoff in a full-scale urban drainage physical model, to be used as the basis for an application of a physically-based sediment wash-off 2D shallow water model. Due to the low depths developed in the laboratory model and the size of the catchment, this study focuses firstly on measuring a high-resolution topographic data using a low-cost photogrammetric technique, allowing thus for the proper simulation of the surface flow with a 2D shallow water model. Then, a hydraulic experimental characterization of the runoff is measured under controlled laboratory conditions to calibrate and assess the numeric results obtained. The maximum depths of around 5-8 mm, and the presence of raindrops that interfere in the visualization of the surface flow, made it necessary to develop a modified LSPIV methodology using fluorescent particles. To the authors' knowledge, no previous urban drainage studies have applied LSPIV during rainfall events. Therefore, the present study is novel in the following ways:

- The SfM technique is used to obtain a high-resolution and accurate elevation map of an urban drainage physical model of 36 m^2.
- Extreme-shallow surface flow is measured in the presence of raindrops with a modified LSPIV methodology, by means of fluorescent particles.
- The photogrammetric topography and a traditional topographic survey using a gridded system have been implemented in a 2D shallow water model in order to validate both digital terrain models with the measured LSPIV velocity fields.

2. MATERIALS AND METHODS

2.1. Physical model description

Experimental testing was undertaken in the Hydraulic Laboratory of the Centre of Technological Innovation in Construction and Civil Engineering (CITEEC) at the University of A Coruña. The installation consists of a full-scale street section with a rainfall simulator located 2.6 m over a 36 m^2 concrete street surface, divided into a tiled pavement and a roadway (Figure 1). The runoff generated by rain drains into a sewer drainage system by means of three gully pots, two of these located along the curb and a third one at the end of a lateral outflow channel. The gully pot grate was removed in the tests to allow sampling of water quality parameters in them in a series of wash-off experiments not shown here. The surface has an approximate transversal slope of 2% up to the 0.15 m high concrete curb and a 0.5% longitudinal slope up to the outflow channel. A more detailed description of the physical model can be found in Naves et al. (2017).

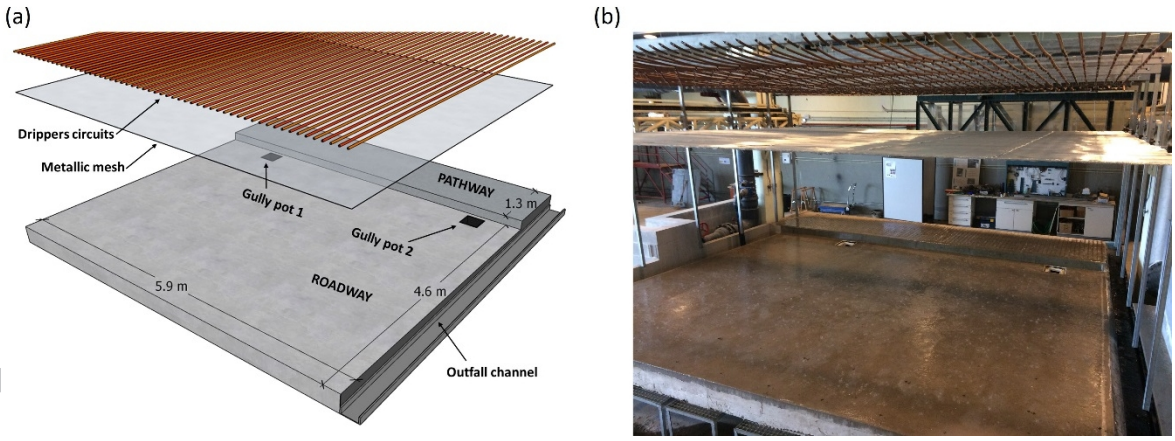

Figure 1. (a) Physical model scheme and (b) general image of the facility.

The rainfall simulator consists of two overlapped circuits of pipes with pressure-compensating irrigation drippers (PCJ-CNL, Netafim™) inserted in a grid layout. The transversal and longitudinal distance between drippers in each circuit is 0.2 m (25 drippers per square meter) and the flow generated by one dripper is 1.2 and 2 L/h,

respectively. This configuration makes it possible to simulate rainfall with a rain intensity of 30 mm/h, 50 mm/h and, if both circuits are used at the same time, 80 mm/h. A metallic welded wire mesh with 3 mm square openings, situated 0.6 m below the grids of drippers, breaks and distributes the generated raindrops to achieve a suitable uniformity and drop size distribution. The rain intensity distribution was measured from the volume collected in a 0.5 m x 0.5 m grid of vessels for 5 minutes. The obtained Christiansen Uniformity Coefficients (Christiansen, 1942) values for 30 mm/h, 50 m/h and 80 mm/h were 76%, 88% and 91%, respectively; hence, the rain can be considered almost uniform.

2.2. Surface model topography

2.2.1. Traditional point data survey

The 3D coordinates of a total of 144 points were determined over the whole surface of the physical model in a 0.5 m x 0.5 m grid. The x- and y-coordinates of each point of the grid were determined by triangulation from two reference points, while the z-coordinate was obtained by measuring the distance to a horizontal reference laser plane with a point gage tape. The error bounds of the measured horizontal coordinates were assumed to be approximately 1 cm for the horizontal coordinates, and about 1 mm for the vertical coordinates (Boiten, 2003). The position of the points used for the topographic survey was drawn over the street surface with red crosses (see Figure 4). These marks were also used as reference points in the visualization techniques carried out in this study.

2.2.2. Structure from Motion survey

The SfM photogrammetric technique was applied to obtain a high-resolution elevations map of the physical model surface. The first step was to take a total of 64 images from different positions around the surface with a Lumix GH4 camera (focal length equal to 28 mm and image resolution 3264x2448 pixels). Then, the free license

software VisualSFM (Wu et al., 2011, Wu, 2013) was used to perform the 3D reconstruction of the physical model surface. This software uses triangulation to obtain the relative position of different features of the studied object which appear in several images at the same time. Therefore, it is necessary to ensure an overlap of the images of around 60 % to increase the number of resulting points. In addition, enough contrast in the surface of the measured object is also needed in order to distinguish and correlate the common points between the images. In this particular case, the concrete surface is very homogeneous and it was no possible to apply directly the SfM technique because the software cannot identify different features in the pictures. To avoid this problem, a colored and texturized image was projected over the surface of the model while the images were taken, and in this way a sufficiently dense point cloud was obtained (Figure 2).

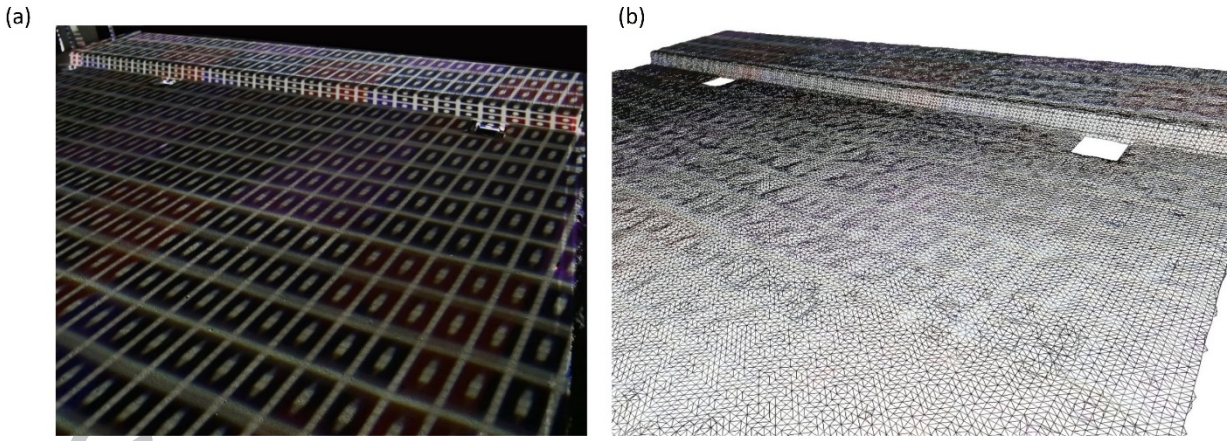

Figure 2. (a) Texturized image projection over the street surface used for the application of SfM and (b) 3D dense point reconstruction of the model.

A ~976,000 elements dense point cloud in a relative coordinate system was obtained by means of the SfM technique. A total number of 5 ground reference points, previously determined in the traditional data topographic survey, were used to scale and transform the point clouds to a coordinate system that was already known. This procedure was carried out with the open source software Meshlab (Cignoni et al.,

2008). The RMSE resulting from the differences between the final coordinates and the calibration ground points was 2.2 mm. Finally, the Screened Poisson Surface Reconstruction in Meshlab (Kazhdan and Hoppe, 2013) and a 40 x 60 elements two-dimensional median filter method was applied to the scaled and positioned point cloud in order to obtain a 5 mm squared despiked grid.

2.3. Numerical model

The Iber model (www.iberaula.es) was used to assess the effect of the different measured topographies in the overland flow velocity distribution and flow discharges into the model gully pots. The surface drainage model solves the 2D shallow-water equations, including rainfall and infiltration terms, with an explicit un-structured finite volume solver. The model has been validated in previous studies under overland flow conditions including rainfall-runoff transformation (Cea et al., 2010, Cea and Blade 2015). The surface runoff model Iber has also been implemented in the dual drainage model of the authors' research team, which has already been validated in field applications (Fraga et al. 2016) and in the same physical model presented in this study (Fraga et al. 2015). A detailed and comprehensive description of the numerical model and solver can be found in the previously cited studies. Following Fraga et al. (2015), all the boundary conditions of the model were imposed as free critical depth discharge. In the present study, gully pots were not treated with any special stage-discharge curve, as the gully pots grates were removed.

2.4. Determination of overland flow velocity fields

The LSPIV technique was used to obtain the velocity field of the superficial flow within the first two meters of the pavement placed next to the curb of the physical model. This area presents the highest depths and velocities due to the transversal slope of the street model, and it is the most interesting part from an urban wash-off point of view since it is known that most of the sediments build up in the first 0.5 m

(Sartor and Boyd, 1972, Grottker, 1987). LSPIV are based on the analysis of the frames obtained from a video recording of some type of tracer that is supposed to follow the velocities of the superficial flow, so the selection of a suitable tracer and the correct way of recording the video are essential before beginning the experiments.

2.4.1. Experimental setup

Two Lumix GH4 cameras were used to apply the LSPIV technique. Both cameras used a focal length of 28 mm and were set to record video frames of size 3840x2178 pixels and a frame rate of 25 Hz. The cameras were positioned 2.2 m above the side of the pathway. The camera configuration ensures the detection of small particles around 1 mm diameter and allows for the recording of an area large enough to capture the half length of the physical model curb (Figure 3).

The conditions of the experiments must be taken into account in the selection of the particles used as a tracer. First, the particles have to be small and light enough to be transported by the flow considering the low depths developed in the surface of the physical model. The maximum depths for the maximum rain intensity are below 10 mm next to the curb and around 3 mm on the rest of the surface. Furthermore, the presence of raindrops between the cameras and the water surface and their impacts on it produces different image patterns that affect the accuracy of PIV algorithms, which are not able to distinguish between tracers and these other picture features. To deal with this problem, fluorescent ultraviolet (UV) particles and lamps were used to illuminate the physical model. Fluorescent particles have been used in the past in PIV applications to improve the quality of the acquired images, allowing measurements close to laser-reflective surfaces such as sediment beds or free surfaces (Pedochi et al. 2008). In our study we produce inexpensive LSPIV particles by cutting an extruded 3D-printer fluorescent strand into pieces. These fluorescent particles (0.85 mm mean size) react with the shining UV light, so that in dark conditions it is possible to highlight the particles, distinguishing them from the rest of the disturbing features in the images,

such as raindrops or water reflections. Therefore, five UV 100 LED torches (390 nm wavelength) were placed next to the cameras and pointing at the surface in order to illuminate homogeneously the measured surface during the experiments. In the Figure 3, a scheme of the experimental setup is shown.

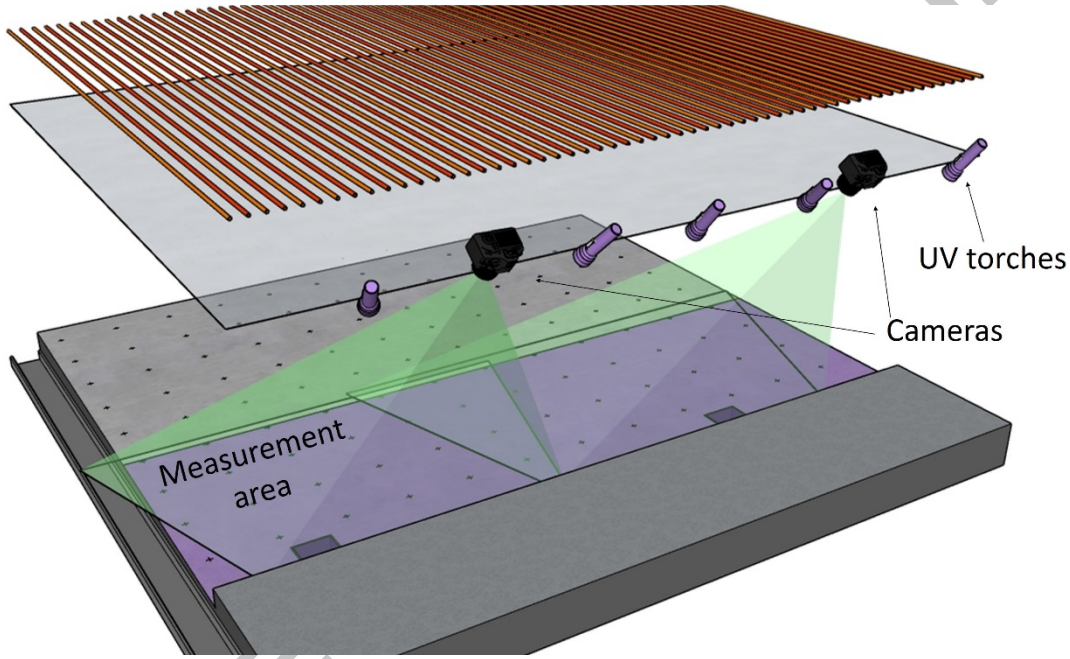

Figure 3. Layout of the experimental configuration for overland runoff velocity measurements in the physical model.

2.4.2. Experimental procedure

For each of the three rain intensities that the rainfall simulator can generate, the measure of the superficial flow by means of the LSPIV technique began by turning off the ambient laboratory lights while the cameras were recording. Then, the UV torches were turned on and the rain started. Once steady conditions were reached, after approximately 150 seconds, particles were spread manually along the side of the roadway during the rest of the experiment, which has a total rainfall duration of 300 seconds. This allows the particles to be transported to the measurement area without causing disturbances in the flow or in the video, and we ensure the recording of at least one minute of a suitable particles flow in steady conditions at the measurement area.

2.4.3. Image processing and LSPIV data analysis

Once the experiment was finished, 1500 frames (60 seconds) were extracted from the video as recorded in steady flow conditions. The frames were processed with the procedure schematized in Figure 5, which consists of the following steps:

Spatial calibration

The angle of view of the cameras and the lens distortion cause a deformation in the video frames recorded, so the extracted frames from the video sequences were dewarped to correct image perspective and to convert the image units from pixels to real world metrics. This procedure was performed using a spatial calibration of the images using the red cross marks drawn on the model surface during the gridded point data topographic survey. The point coordinates were used as a reference to transform the camera frames to an orthogonal Cartesian coordinate system. In each experiment and for each camera, the standard Matlab algorithm 'fitgeotrans' was applied to one frame recorded in normal light conditions. A total number of 28 and 24 reference points with known 2D coordinates were identified in the calibration frame of each camera. The software provided a rototranslation matrix to transform the frames recorded during the experiments. In these new scaled and orthoreferenced images obtained by applying the matrix, 1 pixel corresponds to 1 mm in real-world coordinates. Finally, the common referenced points between the cameras were used to crop and join the image. A similar procedure for image calibration was performed by Arques et al. (2018).

The final position of all the reference points in the calibrated image was compared with the known coordinates, obtaining a maximum error of about 2% in the total displacement between marks. This calibration procedure was applied for each experiment to avoid errors because of possible small movements or tilts of the cameras between experiments. The time synchronization between cameras was done through identifying the frame at the moment that the lights of the laboratory was turned off. The process is very fast and it is easy to identify the first frame recorded in dark

conditions, so this method provided the maximum possible accuracy, which is equal to the time step between frames (0.04 s).

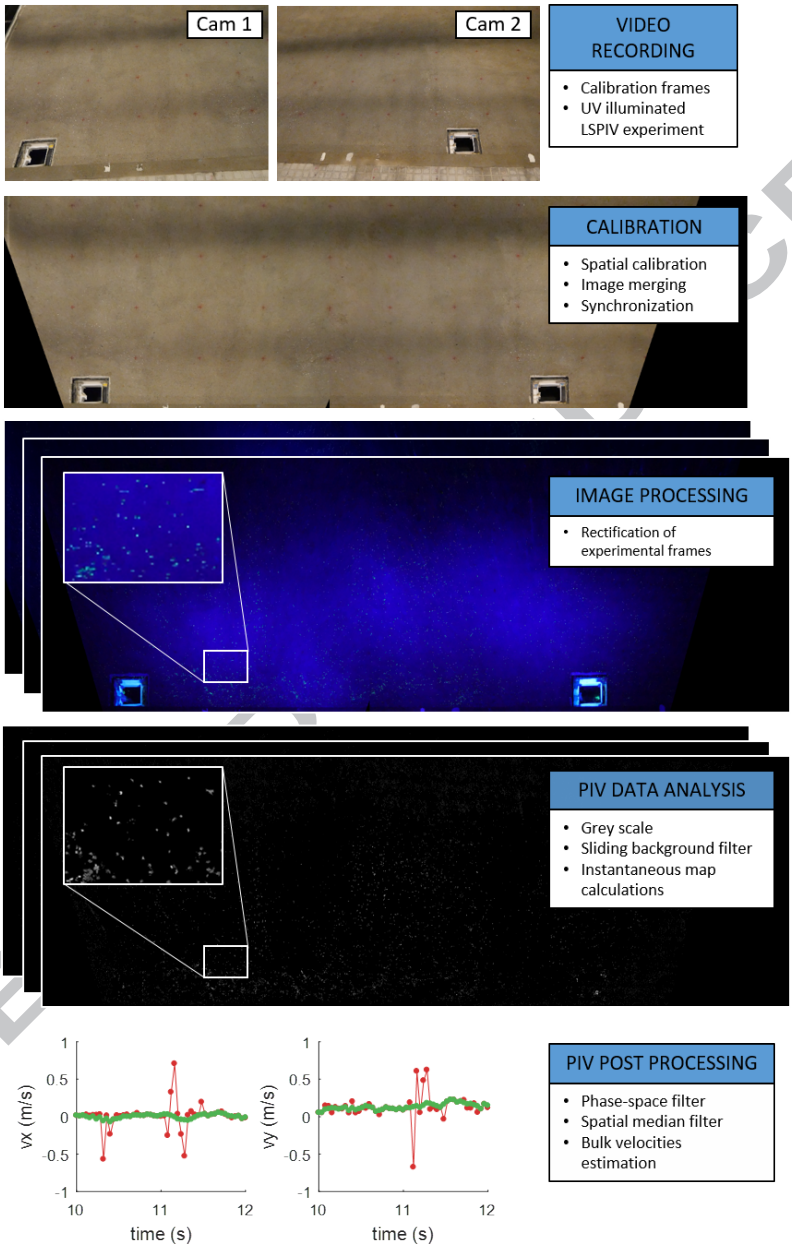

Figure 4. Image processing and LSPIV data analysis methodology

PIV data analysis

Before the application of the PIV cross-correlation algorithms to the recorded images, the rectified and merged images were converted to grey scale, and a moving sliding background with a 0.25 threshold filter was then applied. Thus, in each frame

those pixels with 25 % of similarity in the grey value with the same pixel from the previous frame were transformed to black. The application of the sliding background filter reduces the effect of background image features such as surface microtopography roughness or tracer particles that settled temporarily on the shallowest or dry flow regions. The velocity of these particles would be zero and the mean velocity estimation in the interrogation area is biased.

For the determination of the instantaneous velocity maps the open source PIV tool for Matlab 'PIVLab' (Thielicke and Stamhuis, 2014) was used. An adaptive cross-correlation procedure was performed using squared interrogation areas of 128, 64 and 32 pixels, resulting in a regular grid of velocity vectors of 3.2 cm and 0.04 s of resolution. To estimate the cross-correlation between frames an FFT approach was used, and in the final step a window deformation scheme was applied to increase PIV accuracy (Raffel et al., 2007).

PIV data post-processing and velocity calculation

Once the velocity fields were obtained, the possible outliers were detected with a temporal 2D filter using a phase-space thresholding method developed by Goring and Nikora (2002), taking into account both velocity components in each point throughout the duration of the experiment. The filter removes less than the 8 % of the velocity vectors. Then, these outliers were replaced by means of a linear interpolation following Cea et al. (2007). In Figure 4 (lower part), above, a real example of the performance of the temporal 2D filter in a selected point in one experiment can be seen. Finally, in the Matlab toolbox 'pivmat' environment (Moisy, 2017), a spatial median filter of 3x3 elements was performance to all the frames.

The obtained velocity fields correspond to the surface flow velocity. In order to obtain the mean depth-averaged velocity value, it is necessary to determine a velocity-index or flow velocity correction factor. In river surveys, the determination of the velocity-index is based on the application of the log-law velocity profile to the

streamwise velocities (Le Coz et al., 2010). For the complex shallow flows developed in urban surfaces, this assumption may be questionable, and some authors use different velocity index values ranging roughly from 0.6 to 1 (e.g. Leitao et al. 2018, Martins et al. 2018). Nevertheless, due to the relatively shallow flow depths under consideration, errors arising from this assumption are not expected to be significant, since depth-averaged velocities are relatively small, and other uncertainties related to the methodology may be expected (for instance due to the trapping of seeding particles in the shallowest areas). Taking all these considerations into account, and from a practical point of view, the classical index velocity value of 0.85 was applied in this study.

2.5. Determination of flow discharges

In addition to the surface velocity field, the inflow discharges in the gully pots were measured for the 3 rainfall intensities in order to calibrate the 2D shallow water model. A triangular weir was installed in two underground tanks placed under the gully pots. In each tank an ultrasonic distance sensor (UB500-18GM75-I-V15, Pepperl and Fuchs) was installed in order to measure the flow discharge over the triangular weir. First, the spikes of the 10 Hz raw signal were removed using a moving median filter of 5 seconds, replacing the peaks that overcome the double of the deviation by the median of this range. Then, the flow in the gully pots was obtained by means of a depth-flow pre-calibration and a volume compensation performed because of the changes of depth in the reservoir when the flow is increasing or decreasing. This methodology was described in more detail in Naves et al. (2017).

3. RESULTS AND DISCUSSION

In this section, the surface models from the traditional topographic survey and SfM photogrammetric data are first presented (Section 3.1). Then, we describe how the 2D shallow water model was used to simulate the runoff for 30 mm/h, 50 mm/h and 80

mm/h rain intensities with both topographies (Section 3.2). The measured discharges in physical model gully pots were used to calibrate the numerical model, and the simulated velocity maps are then presented. Finally, the experimental velocities obtained using the LSPIV technique in the physical model are presented and compared with the numerical results (Section 3.3).

3.1. Elevation data and model discretization

The elevation maps of the physical model obtained from the data point and the SfM topographic surveys are shown in Figure 5. Both topographies consist of a regular gridded data at 50 cm spatial resolution and of an SfM topography at 5 mm spatial resolution. The comparison between these elevation maps is focused on the area along the first two meters next to the curb (x=0 m to x=2 m). The elevation of 40 points placed in this region was obtained from both topographies. The RMSE of the elevations was 2.9 mm, indicating a high correlation between the topographies. Therefore, the SfM technique allows us to obtain a similar accuracy with a larger spatial resolution.

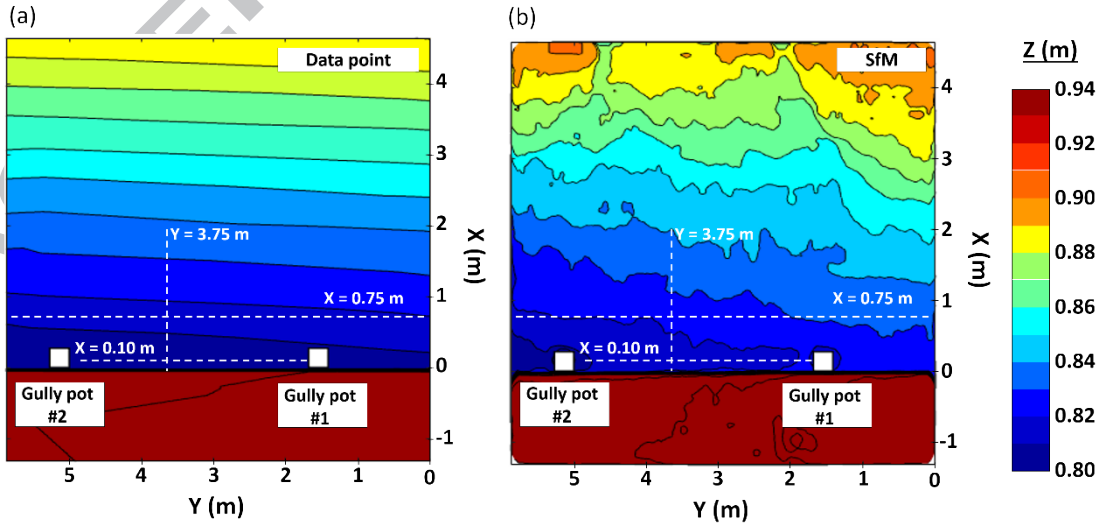

Figure 5. Topographies of the physical model obtained from (a) traditional point survey and (b) SfM photogrammetric technique. Longitudinal and transversal cross section plotted in Figure 6 and 11 are marked in the maps.

The point data surface is smoother than the SfM surface, and as expected from the model description and building specifications, the transversal slope is higher and more uniform than the longitudinal slope. The SfM topography shows a more irregular contour line definition and the presence of small transversal valleys and crests, which serve as drainage channels orthogonal to the curb of the model. As will be shown below, theses surface irregularities found between the manual and SfM surveys affect the modelled runoff velocities, particularly in the case of low depths.

Both topographies were converted to a raster format decimated to a resolution of 5 cm. The model domain discretization was performed using a structured mesh made with triangular elements, with edge sizes ranging from 5 cm to 7 cm. The number of cells of the model is about 58,000 elements and was automatically generated from the raster files using the Iber software (Cea and Blade, 2015). To highlight the differences in the domain discretization, Figure 6 shows a transversal profile at y=3.75 m (upstream of gully pot 2) and two longitudinal profiles placed at x=0.75 and x=0.10 m, representing the surface morphology upstream and between the gully pots, respectively. The gridded data mesh presents a visible quantization error caused by the coarse 50 cm resolution of the original data points. The averaged slope of the profiles determined from the gridded point data and the SfM approach are similar, but the SfM longitudinal profiles show some depressions of few millimeters' depth at x~2.4 m, x~3.3 m, x~4 m and x~4.8 m, which act as drainage channels.

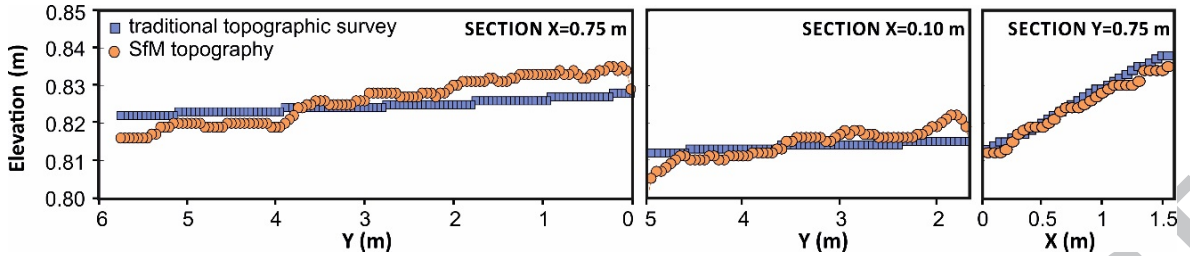

Figure 6. Comparison of the longitudinal (x=0.75 m and x=010 m) and transversal (y=3.75m) profiles extracted from the model domain generated from traditional point data and SfM topographies.

3.2. Application of the 2D shallow water model

The topographies presented in the previous section have been implemented in Iber 2D shallow water model to analyze their influence in modelling the runoff for the three rainfalls here, of 30, 50 and 80 mm/h and 5 minutes' duration. A common calibration dataset for all six cases (two topographies and three rain intensities) was defined in light of the discharges measured in the gully pots of the physical model. A non-formal calibration procedure was performed, changing the Manning coefficient and the initial losses of the concrete surface of the model. An initial loss of 0.6 mm was fixed to assure that modelled and measured runoff volumes were similar. The Manning coefficient was set at 0.016. This value accounts for the extra bed roughness induced by the rainfall. Although the numerical model incorporates a variable-depth Manning formulation, slight improvements with variable roughness parametrization are achieved, this mainly in the recession and rising hydrographs limbs (Fraga et al. 2013), which are not compared with the LSPIV results, as will be shown below. From a practical point of view, a constant roughness parametrization produces results with a similar accuracy to the variable roughness-dependent formulations for the smooth surfaces (Cea et al. 2014).

A visual inspection of Figure 7 reveals a very good fit between the outputs of the numerical model with both topographies and the experimental results using the previous model's inputs. Therefore, if we look only at the discharges into the gully pots,

the manually measured topography has enough resolution to properly model the overland flows, while the SfM topography does not improve model accuracy.

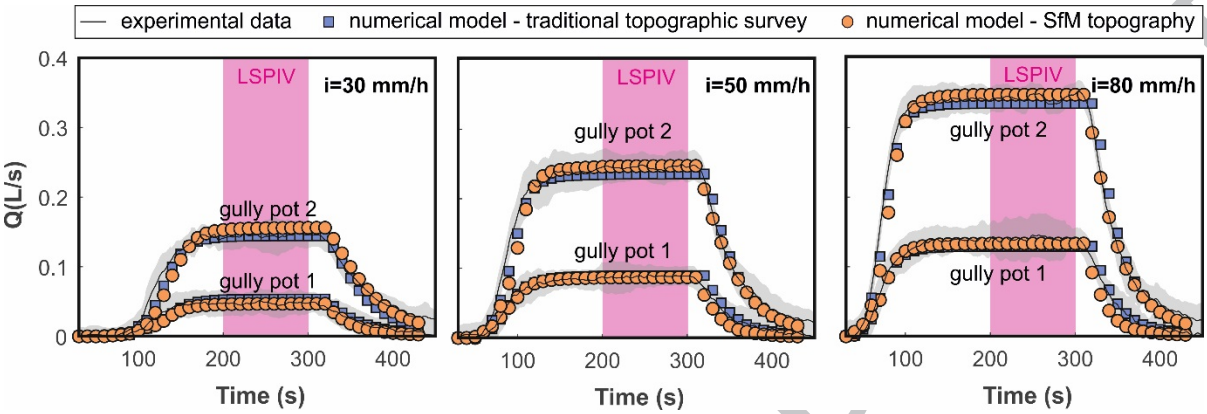

Figure 7. Experimental and numerical flow results in both gully pots and for the three rainfall intensities studied. The variance in the measured experimental flow discharge (grey) and the LSPIV measure interval (purple) are shown.

Figures 8 and 9 present the depth-averaged velocity maps obtained for both topographies in steady conditions (e.g. after 200 seconds from the beginning of the rainfall). As numerical and experimental data do not match exactly, numerical data has been spatially interpolated. Therefore, to clarify the representation of the velocity vectors a spatial resolution of ~16 cm was selected for the graphics.

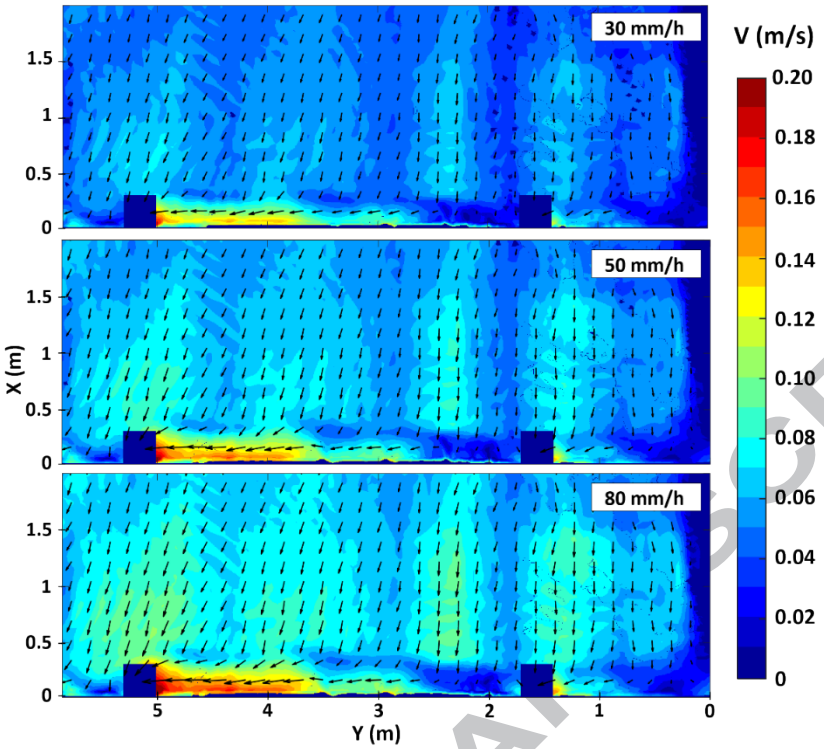

Figure 8. Numerical depth-averaged velocity vectors using the traditional data point topography for 30, 50 and 80 mm/h rainfall intensity.

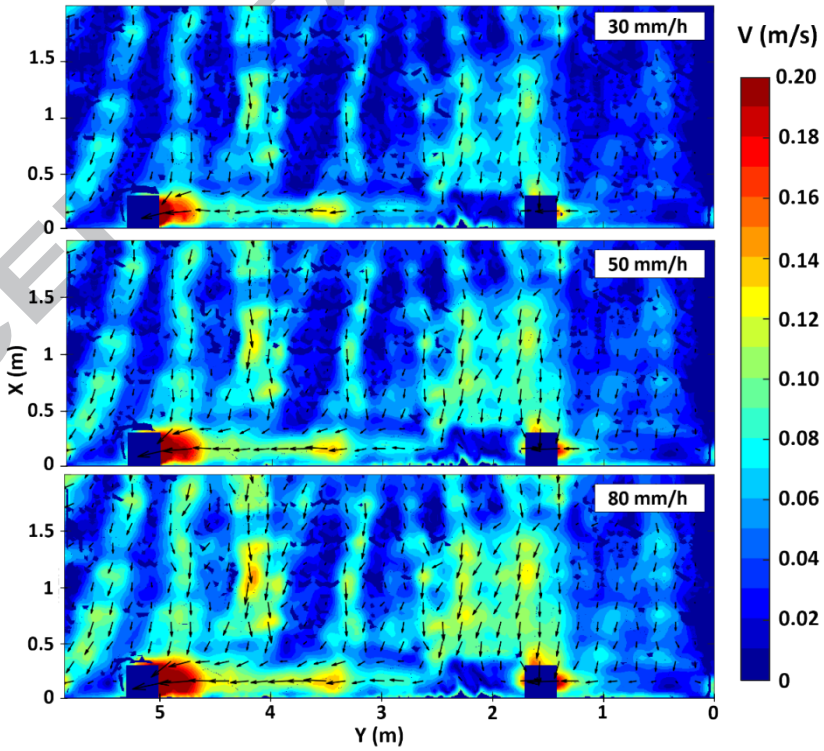

Figure 9. Numerical depth-averaged velocity vectors using the SfM topography for 30, 50 and 80 mm/h rainfall intensity.

Regarding the general flow patterns, in both model domains the runoff drains towards the two gully pots and the curb, due to the transversal and the longitudinal slope, but some preferential channel flows orthogonal to the curb direction appear when the SfM elevation map is used (Figure 9). Although these preferential channel flows could also be sensed by using the manually measured topography, the higher resolution of the SFM technique results in far better defined drainage channels, where the velocities are roughly five times the velocities in the areas between them. Furthermore, the width and mean velocity of these transversal channels increased with rainfall intensity.

Another difference observed in the flow pattern determined using each topography is related to a velocity reduction of the curb channel flow at the junctions with the transversal drainage channels. This effect is more pronounced in SfM model domain at y~4 m, where the more defined orthogonal junction between transversal and longitudinal overland flows produces a decrease in the average velocity of the curb flow. In addition to these differences, the overland flow obtained with the SfM model domain presents some areas with dry fronts due to the high sensitivity to the surface elevations variability in the shallowest depth conditions presented far away from the model curb.

Thus, considering the suitable performance of the manual gridded point data and SfM topographies for modelling gully pot discharges, it becomes necessary to asses with experimental velocity data which approach gives a better representation of the runoff flow patterns. This assessment will be performed using LSPIV data in the following section.

3.3. Application of LSPIV to determine overland flow velocities

As mentioned in the section on methodology, the surface velocities determined by applying the LSPIV technique with fluorescent particles were converted to depth-

averaged velocities by applying a velocity index of 0.85. Figure 10 shows the vector field for the rainfall intensities of 30, 50 and 80 mm/h represented with the same spatial resolution as Figures 8 and 9. The orthogonal channels to the curb which were found by using the SfM topography appear clearly in the experimental results. Furthermore, the decrease in the velocities in the junctions between the main transversal and the longitudinal flow channels noted in the previous section is also well registered by the experimental data. Regarding the velocities, it can be noted that the LSPIV and numerical results for SfM are of the same order of magnitude.

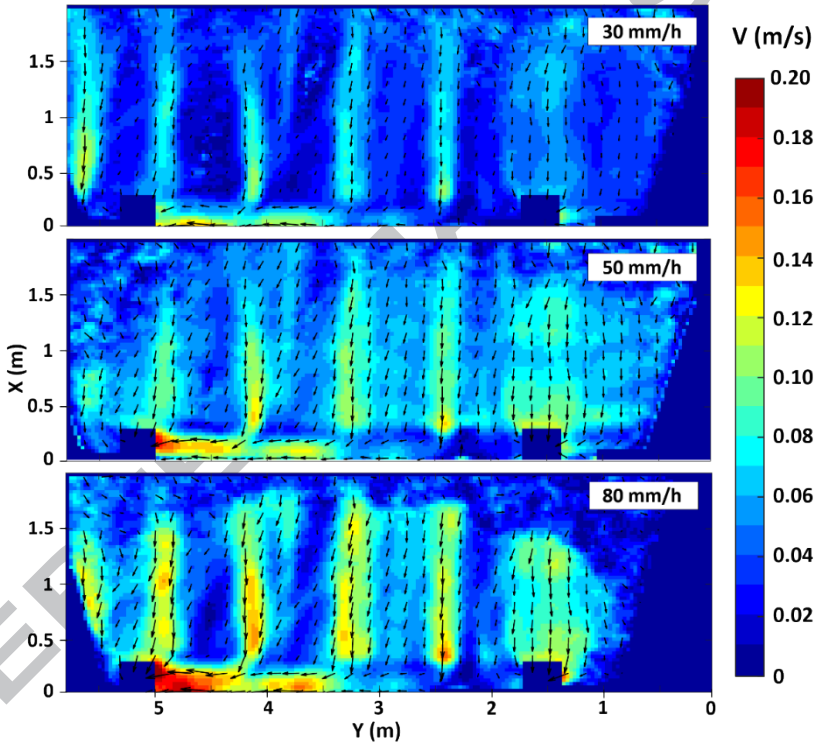

Figura 10. Experimental surface velocity fields for the three studied rainfalls using LSPIV.

From the results obtained in Figure 10, it can be seen that the LSPIV methology developed in this study appears to be a suitable tool for measuring overland flow velocities over very shallow water depth conditions, in an area larger than 10 m^2 , and avoiding the presence of raindrop features in the recorded images using fluorescent particles. In addition, the importance of the UV illumination is noted in the furthest

regions from the camera and torch positions, where the higher the rain intensity the less accurate are the measurements (e.g. $y < 1$ m, $x > 1.6$ m). This is caused by the interference of the raindrops with the light from the torches and the video recording, so a brighter UV illumination should be considered in the case of larger areas being measured.

The match between the experimental results and the velocity fields obtained using both topographies have been investigated in the comparison carried out for each velocity component in Figure 11. The comparison was limited to the area between gully pots and up to 1.5 m from the curb, this to avoid the area where the LSPIV measurements are less accurate due to irregular illumination. Firstly, a clearly different performance can be observed in the comparison of the LSPIV x-velocities with both numerical results. These x-velocities correspond to the flow transverse to the curb, where the drainage channels have been measured with the LSPIV technique. While the numerical results obtained using the traditional point data topography have an almost constant value, ranging from 0.05 to 0.08 m/s for the three rain intensities studied, the SfM topography results are distributed in the range of variation of the experimental velocities (e.g. following the 1:1 slope relationship). This bias in the velocity distribution using the conventional topography is due to the fact that, with the lower resolution associated with this topography, the model is not able to reproduce the drainage channels and a homogeneous velocity results for all of this area. Regarding y-velocities, which correspond roughly to the curb flow, both implemented topographies showed similar results, with a slight increase of the dispersion in the case of those obtained using the SfM topography.

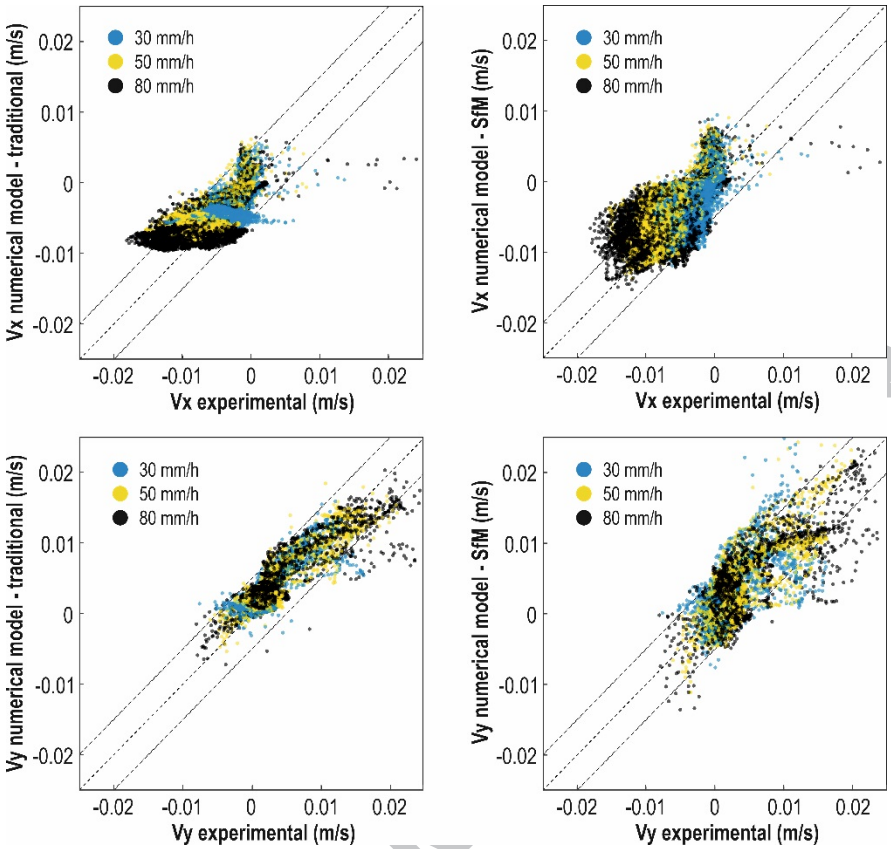

Figure 11. Comparison of the experimental and numerical x-component (up) and y-component (down) velocities using the experimental data obtained from the LSPIV technique and the numerical results, with the traditional point data topography (left) and the SfM topography (right), respectively. The three different rainfall intensities of 30 mm/h, 50 mm/h and 80 mm/h are represented in blue, yellow and black.

Figure 12 presents the results as a histogram for each velocity component of the experimental data and the empirical probability density function obtained with the point data and SfM topographies for the three different rainfall intensities. It can be seen that the distribution of the x-velocity component and mean velocities is better represented with the SfM numerical model. When comparing the velocity histograms (Figure 12a and 12b), we can see that they have a similar shape, which points to a good relation between experimental and numerical results obtained with the SfM topography. The velocity distribution obtained with the traditional topographic survey model is concentrated in the range of 0.05 – 0.10 m/s due the inaccurate representation of the

drainage channels placed in a transversal direction to the physical model curb. For the longitudinal velocity component (Figure 12b), both numerical probability density functions have a similar shape, although the calculated SfM presents a slightly larger dispersion than the gridded data values, as is shown in the lower part of Figure 11 (above).

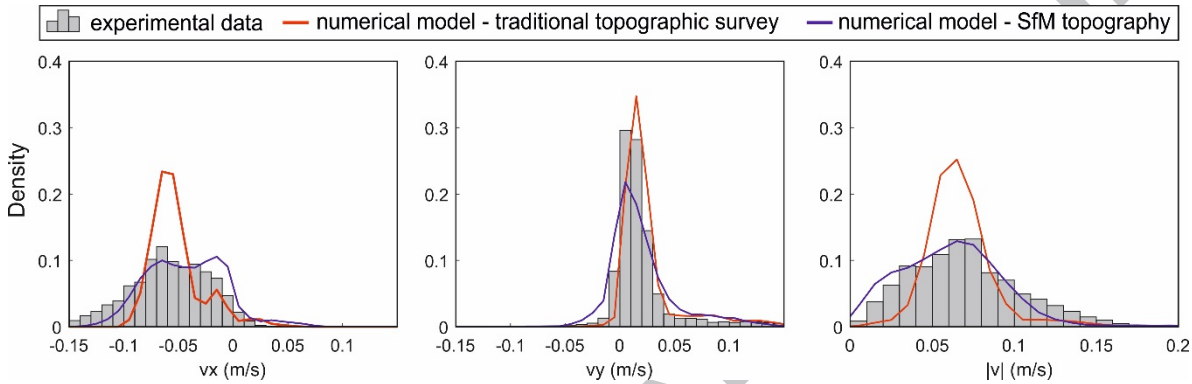

Figure 12. Density comparison (histograms) for x-component (a) y-component(b) and module (c) of experimental and numerical velocities.

In order to check and understand the different results obtained in the comparison of numerical and experimental data, depth-averaged (mean) velocity has been plotted in three sections of the model in Figure 13. The chosen sections are intended to represent the different types of flows over the physical model surface: first, a longitudinal section (x=0.75 m) has been selected to compare the velocities distribution in the region of the drainage channels and to check how the higher resolution of the SfM topography allows us to represent channel velocity variation in the transversal flow; furthermore, an aditional longitudinal section (x=0.10 m) and a cross-section in y=3.75 m have been used to assess the curb flow and investigate the higher dispersion shown in Figure 11 and 12 in the case of the SfM topography, despite its higher resolution. The uncertainty in the LSPIV experimental results has been included by plotting the standard deviation of the measured velocities in the recorded interval.

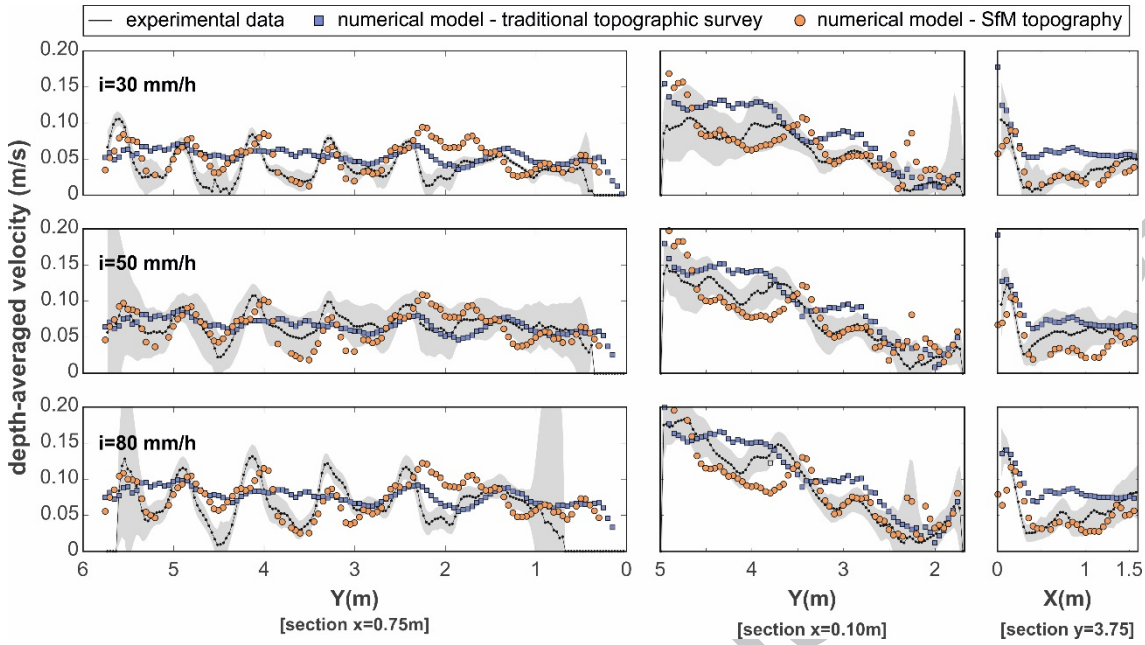

Figure 13. Numerical and experimental depth-averaged velocity sections comparation (X=0.75 m, X=0.10 m and Y=3.75 m) for the three rainfall intensities studied.

Looking at the first section (x=0.75 m) for all the rain intensities in Figure 11, it can be noted that the numeric results from the point data measured topography is not able to simulate the drainage channels and keep an almost constant velocity value over the cross-section, especially between y~5.5 m and y~2 m. However, the model with the SfM elevations shows a reasonable agreement with the experimental data and fits the peaks where the velocity increases in the drainage channels, with the exception to region ranging from y~1 to y~2 m. The standard deviation of the experimental velocity is about 0.01 – 0.02 m/s, except for the bounds of the visualization domain, where higher experimental errors are expected due to insufficient illumination.

In the case of the second section (x=0.10 m), the influence of the topography in the numeric results is apparently lower due to the higher flow depth developed next to the curb. But although both numeric results simulate satisfactorily the increasing tendency of the curb flow velocity between the gully pots, the SfM model is able to follow the shape of the velocity changes produced in the junctions between the transversal channels with the curb flow, a slight variation of position being observed in

the velocity peak around y=3.5 m. Finally, the last transversal section shows a limitation of the SfM technique measuring the elevations of roughly the first centimeters next to the curb, in that we can see the reduction of the velocities around this area compared with the manual topographic survey and the experimental results. These two discrepancies observed in the curb flow could explain the higher disparity presented by the y-velocities from the SfM topography with respect to the experimental data observed and commented on in Figure 11. However, the photogrammetric technique provides a better fit in the rest of the section, confirming their better performance in modelling the runoff that has been shown above.

Overall, it can be concluded that the SfM model has a higher correlation with the experimental measurements. The results obtained with the SfM domain represent accurately the qualitative flow behavior, although some quantitative differences have been highlighted in the position of some of the peaks of the cross-sectional velocity profiles. These differences could be attributed to errors in the determination of the elevation maps or in the determination of the velocity fields. The errors related to the topography are more relevant in the areas with lower depths and close to the curb edge. The errors in the velocity determinations are mainly located in some specific areas of the model due to a poor local particle illumination, or related to the shallow water conditions tested in this study, commonly lower than 1 cm. In these conditions tracer particles can eventually settle, as they can be trapped by pavement surface irregularities, thus affecting the determined magnitude of the velocity vectors.

4. CONCLUSIONS

In this study, novel techniques such as SfM photogrammetry and a modified LSPIV were applied in order to obtain, using a 2D shallow water model, an accurate representation of the overland runoff generated by three different rain intensities, of 30, 50 and 80 mm/h, in an urban drainage physical model. Based on the results, the following conclusions can be drawn:

- The SfM photogrammetric technique provided a fast and effective way to obtain an elevation map that differed in a RMSE error of 2.9 mm from the traditional topographic survey coordinates of a regular rectangular grid of 0.5 m x 0.5 m, but with a spatial resolution 100 times higher.
- The modelled discharges into the gully pots obtained with a 2D shallow water model with gridded and with SfM topographies are almost identical. However, clear differences appear when the overland velocity fields are compared. The differences are due to the far higher spatial resolution of the SfM survey, revealing the existence of drainage channels of a few milimeters' depth placed orthogonally to the model curb. In these drainage channels the local velocities increased due to the small-scale irregularities of the surface.
- By means of fluorescent particles and UV illumination, LSPIV was presented as a very useful non-intrusive tool to accurately measure surface flow velocities in shallow water conditions of few milimeters' depth with a high spatial resolution, including the longitudinal and transversal channel curb flow, in a medium-size area of around 10 m^2, and avoiding the presence of raindrops that might interfere in the measurements.

Thus, this study highlights not only the great value of the topographic modelling of surface flow in shallow water conditions and the importance of a detailed elevation map, but also the need for additional surface velocity calibration data as well as the register of hydraulic variables in the sewer network to achieve useful and accurate surface flow results. Furthermore, the findings of this study are intended to contribute to the development and improvement of new affordable techniques to measure these essential data and to be able to obtain a suitable surface flow representation to be used as the basis for wash-off and flood risk assessment studies in urban catchments.

Acknowledgments

This work was partially supported by the Spanish Ministry of Science, Innovation and Universities [grant number UNLC15-DE-2862, CGL2015-69094-R MINECO/FEDER, UE]. The first author was in receipt of a Spanish Ministry of Science, Innovation and Universities predoctoral grant [FPU14/01778]. The authors would also like to acknowledge the support of Esteban Sañudo in the development of experiments, and the fruitful discussions with Luis Cea, Beatriz Náscher and Paco Vallés.

References

Adrian, R.J., 1991. Particle-imaging techniques for experimental fluid mechanics. Annual review of fluid mechanics. 23 (1), 261–304. https://doi.org/10.1146/annurev.fl.23.010191.001401.

De Almeida, G. A., Bates, P., & Ozdemir, H. (2018). Modelling urban floods at submetre resolution: challenges or opportunities for flood risk management? Journal of Flood Risk Management, 11, S855-S865. https://doi.org/10.1111/jfr3.12276

Arques, S.R., Rubinato, M., Nichols, A., Shucksmith, J.D., 2018. Cost effective measuring technique to simultaneously quantify 2D velocity fields and depth-averaged solute concentrations in shallow water flows. Flow Meas. Instrum. 64, 213–223. https://doi.org/10.1016/j.flowmeasinst.2018.10.022.

Boiten, W., 2003. Hydrometry: IHE Delft Lecture Note Series. 1st Ed. CRC Press, ISBN 9789054104230.

Branisavljević, N., Prodanović, D., 2006. Large Scale Particle Image Velocimetry – merenje urbanog oticaja (in Serbian). Vodoprivreda. 38 (4–6), 233–238. Available

at: http://www.vodoprivreda.net/large-scale-particle-image-velocimetry-merenjeurbanog-oticaja/ [Accessed: 28 Dec 2018].

Cea, L., Blade, E., 2015. A simple and efficient unstructured finite volume scheme for solving the shallow water equations in overland flow applications. Water Resour. Res. 51 (7), 5464–5486.

Cea, L., Legout, C., Darboux, F., Esteves, M., & Nord, G. (2014). Experimental validation of a 2D overland flow model using high resolution water depth and velocity data. Journal of hydrology, 513, 142-153. https://doi.org/10.1016/j.jhydrol.2014.03.052

Cea, L., Puertas, J., Pena, L., 2007. Velocity measurements on highly turbulent free surface flow using ADV. Exp Fluids. 42 (3), 333–348. https://doi.org/10.1007/s00348-006-0237-3.

Cea, L., Garrido, M., Puertas, J., 2010. Experimental validation of two-dimensional depth-averaged models for forecasting rainfall–runoff from precipitation data in urban areas. J. Hydrol. 382 (1), 88–102.

Chen, J., Hill, A.A., Urbano, L.D., 2009. A GIS-based model for urban flood inundation. J. Hydrol. 373 (1–2), 184–192.

Christiansen, J.E., 1942. Irrigation by sprinkling. Bulletin 670. Publisher: Agricultural Experiment Station. Berkeley, CAL, USA.

Cignoni, P., Callieri, M., Corsini, M., Dellepiane, M., Ganovelli, F., Ranzuglia, G., 2008. Meshlab: an open-source mesh processing tool. In: Eurographics Italian Chapter Conference (V. Scarano, R. De Chiara, U. Erra), Pisa, Italy. 129–136.

Deletic, A., Maksimovic, C., Ivetic, M., 1997. Modelling of storm wash-off of suspended solids from impervious surfaces. J. Hydraul. Res. 35 (1), 99–118. https://doi.org/10.1080/00221689709498646.

Detert, M., Johnson, E.D., Weitbrecht, V., 2017. Proof-of-concept for low-cost and non-contact synoptic airborne river flow measurements. Int. J. Remote Sens. 38 (8–10), 2780–2807. https://doi.org/10.1080/01431161.2017.1294782.

Egodawatta, P., Thomas, E., Goonetilleke, A., 2007. Mathematical interpretation of pollutant wash-off from urban road surfaces using simulated rainfall. Water Res. 41 (13), 3025–3031. https://doi.org/10.1016/j.watres.2007.03.037.

Fraga, I., Cea, L., & Puertas, J. (2013). Experimental study of the water depth and rainfall intensity effects on the bed roughness coefficient used in distributed urban drainage models. Journal of hydrology, 505, 266-275. https://doi.org/10.1016/j.jhydrol.2013.10.005

Fraga, I., Cea, L., Puertas, J., 2015. Validation of a 1D-2D dual drainage model under unsteady part-full and surcharged sewer conditions, Urban Water J. 14 (1), 74–84. https://doi.org/10.1080/1573062X.2015.1057180.

Fraga, I., Cea, L., Puertas, J., Suárez, J., Jiménez, V., Jácome, A., 2016. Global Sensitivity and GLUE-Based Uncertainty Analysis of a 2D-1D Dual Urban Drainage Model. J. Hydrol. Eng. 21 (5), 04016004. https://doi.org/10.1061/(asce)he.1943-5584.0001335.

Fujita, I., Muste, M., Kruger, A., 1998. Large-scale particle image velocimetry for flow analysis in hydraulic engineering applications. J Hydraul. Res. 36 (3), 397–414. https://doi.org/10.1080/00221689809498626.

Goring, D.G., Nikora, V.I., 2002. Despiking acoustic Doppler velocimeter data. J Hydraul Eng. 128 (1), 117–126.

Grottker, M., 1987. Runoff quality from a street with medium traffic loading. Sci. Total Environ. 59, 457–466.

Guillén, N.F., Patalano, A., García, C.M., Bertoni, J.C., 2017. Use of LSPIV in assessing urban flash flood vulnerability. Nat. Hazards. 87 (1), 383–394. https://doi.org/10.1007/s11069-017-2768-8.

Hairsine, P.B., Rose, C.W., 1992a. Modeling water erosion due to overland flow using physical principles: 1. Sheet flow. Water Resour. Res. 28, 237–243. http://doi.org/10.1029/91wr02380.

Hairsine, P.B., Rose, C.W., 1992b. Modeling water erosion due to overland flow using physical principles: 2. Rill flow. Water Resour. Res. 28, 245–250. http://doi.org/10.1029/91wr02381.

Hong, M., Bonhomme, C., Le, M.H., Chebbo, G., 2016a. A new approach of monitoring and physically-based modelling to investigate urban wash-off process on a road catchment near Paris. Water Res. 102, 96–108, https://doi.org/10.1016/j.watres.2016.06.027.

Hong, M., Bonhomme, C., Le, M.H., Chebbo, G., 2016b. New insights into the urban washoff process with detailed physical modelling. Sci. Total Environ. 573, 924–936. https://doi.org/10.1016/j.scitotenv.2016.08.193.

Hunter, N.M., Bates, P.D., Neelz, S., Pender, G., Villanueva, I., Wright, N.G., Liang, D., Fal- coner, R.A., Lin, B., Waller, S., Crossley, A.J., Mason, D.C., 2008. Benchmarking 2D hy- draulic models for urban flooding. Proceedings of the Institution of Civil Engineers - Water Management, 161 (1), 13–30. https://doi.org/10.1680/wama.2008.161.1.13.

Kantoush, S.A., De Cesare, G., Boillat, J.L., Schleiss, A.J., 2008. Flow field investigation in a rectangular shallow reservoir using UVP, LSPIV and numerical modelling. Flow Meas. Instrum. 19 (3–4), 139–144. https://doi.org/10.1016/j.flowmeasinst.2007.09.005.

Kazhdan, M., Hoppe, H., 2013. Screened poisson surface reconstruction. ACM Trans. Graph. 32 (3), 29. https://doi.org/10.1145/2487228.2487237.

Le Coz, J., Hauet, A., Pierrefeu, G., Dramais, G., Camenen, B., 2010. Performance of image-based velocimetry (LSPIV) applied to flash-flood discharge measurements in Mediterranean rivers. J. Hidrol. 394 (1–2), 42–52. https://doi.org/10.1016/j.jhydrol.2010.05.049.

Leandro, J., Chen, A.S., Djordjević, S., Savić, D.A., 2009. Comparison of 1D/1D and 1D/2D coupled (sewer/surface) hydraulic models for urban flood simulation. J. Hydraul. Eng. 135 (6), 495–504. https://doi.org/10.1061/(asce)hy.1943-7900.0000037.

Leitão, J.P., Peña-Haro, S., Lüthi, B., Scheidegger, A., de Vitry, M.M., 2018. Urban overland runoff velocity measurement with consumer-grade surveillance cameras and surface structure image velocimetry. J. Hydrol. 565, 791–804. https://doi.org/10.1016/j.jhydrol.2018.09.001.

Raffel, M., Willert, C., Kompenhans, J., 2007. Particle Image Velocimetry: A Practical Guide. Springer, Berlin, Germany.

Martínez-Gomariz, E., Gómez, M., Russo, B., 2016. Experimental study of the stability of pedestrians exposed to urban pluvial flooding. Nat. Hazards. 82 (2),1–20. https://doi.org/10.1007/s11069-016-2242-z.

Martínez Gomariz, E., Gómez, M., Russo, B., Sánchez, P., & Montes, J. A. (2017). Metodología para la evaluación de daños a vehículos expuestos a inundaciones en zonas urbanas. Ingeniería del agua, 21(4), 247-262. https://doi.org/10.4995/ia.2017.8772

Martínez-Gomariz, E., Gómez, M., Russo B., Sánchez, P., Montes, J.A., 2018. Methodology for the damage assessment of vehicles exposed to flooding in urban areas. J. Flood Risk Manag. e12475. https://doi.org/10.1111/jfr3.12475.

Martins, R., Rubinato, M., Kesserwani, G., Leandro, J., Djordjević, S., Shucksmith, J.D., 2018. On the characteristics of velocities fields in the vicinity of manhole inlet grates during flood events. Water Resour. Res. 54. https://doi.org/10.1029/2018WR022782.

Moisy, F., 2017. PIVMat. Available at: http://www.fast.u-psud.fr/pivmat/ [Accessed: 28 Dec 2018].

Muste, M., Ho, H.-C., Kim, D., 2011. Considerations on direct stream flow measurements using video imagery: outlook and research needs. J. Hydro-environ. Res. 5 (4), 289–300. https://doi.org/10.1016/j.jher.2010.11.002.

Muthusamy, M., Tait, S., Schellart, A., Beg, M.N.A., Carvalho, F.R. de Lima, J.L.M.P., 2018. Improving understanding of the underlying physical process of sediment wash-off from urban road surfaces. J. Hydrol. 557, 426–433, https://doi.org/10.1016/j.jhydrol.2017.11.047.

Naves, J., Jikia, Z., Anta, J., Puertas, J., Suárez, J., Regueiro-Picallo, M., 2017. Experimental study of pollutant washoff on a full-scale street section physical model. Water Sci. Technol. 76 (10), 2821–2829. https://doi.org/10.2166/wst.2017.345.

Neal, J.C., Bates, P.D., Fewtrell, T.J., Hunter, N.M., Wilson, M.D., Horritt, M.S., 2009. Distributed whole city water level measurements from the Carlisle 2005 urban flood event and comparison with hydraulic model simulations. J. Hydrol. 368 (1–4), 42-55.

Novak, G., Rak, G., Prešeren, T., Bajcar, T., 2017. Non-intrusive measurements of shallow water discharge. Flow Meas. Instrum. 56, 14–17. https://doi.org/10.1016/j.flowmeasinst.2017.05.007.

Pedocchi, F., Martin, J.E., García, M.H., 2008. Inexpensive fluorescent particles for large-scale experiments using particle image velocimetry. Exp. Fluids. 45 (1), 183–186. https://doi.org/10.1007/s00348-008-0516-2.

Regueiro-Picallo, M., Anta, J., Suárez, J., Puertas, J., Jácome, A., Naves, J., 2018. Characterisation of sediments during transport of solids in circular sewer pipes. Water Sci. Technol. 2017 (1), 8–15. https://doi.org/10.2166/wst.2018.055.

Sartor, J.D., Boyd, G.B., 1972. Water Pollution Aspects of Street Surface Contaminants. EPA-R2-72-081. United States Environmental Protection Agency, Washington, DC, USA.

Seyoum, S.D., Vojinovic, Z., Price, R.K., Weesakul, S., 2011. Coupled 1D and noninertia 2D flood inundation model for simulation of urban flooding. J. Hydraul. Eng. 138 (1), 23–34.

Thielicke, W., Stamhuis, E.J., 2014. PIVlab – Towards User-friendly, Affordable and Accurate Digital Particle Image Velocimetry in MATLAB. J. Open Res. Softw. 2 (1), e30. https://doi.org/10.5334/jors.bl.

Tomanovic, C., Maksimocik, C., 1996. Improved modelling of suspended solids discharge from asphalt surface during storm event. Water Sci. Technol. 33 (45), 365–369. https://doi.org/10.2166/wst.1996.0527.

Weitbrecht, V., Kühn, G., Jirka, G.H., 2002. Large scale PIV-measurements at the surface of shallow water flows. Flow Meas. Instrum. 13 (5–6), 237–245. https://doi.org/10.1016/S0955-5986(02)00059-6.

Westoby, M.J., Brasington, J., Glasser, N.F., Hambrey, M.J., Reynolds, J.M., 2012. 'Structure-from-Motion' photogrammetry: A low-cost, effective tool for geoscience applications. Geomorphology. 179, 300–314. https://doi.org/10.1016/j.geomorph.2012.08.021.

Wijesiri, B., Egodawatta, P., McGree, J., Goonetilleke, A., 2015. Incorporating process variability into stormwater quality modelling. Sci. Total Environ. 533, 454–461. https://doi.org/10.1016/j.scitotenv.2015.07.008.

Wu, C., 2013. Towards linear-time incremental structure from motion. In: 2013 International Conference on 3D Vision3DV, Seattle, WA, USA. Institute of Electrical and Electronics Engineers (IEEE). 127–134.

Wu, C., Agarwal, S., Curless, B., Seitz, S.M., 2011. Multicore bundle adjustment. In: Computer Vision and Pattern Recognition (CVPR), Colorado Springs, CO, USA. Institute of Electrical and Electronics Engineers (IEEE). 3057–3064.

AUTHOR CONTRIBUTION STATEMENT

Juan Naves: Investigation, Writing-Original draft preparation

Jose Anta: Conceptualization, Writing-Reviewing and Editing, Supervision

Jerónimo Puertas: Conceptualization, Resources, Supervision

Manuel Regueiro-Picallo: Investigation, Visualization

Joaquín Suárez: Conceptualization, Methodology, Resources

Declaration of interests

☒ The authors declare that they have no known competing financial interests or personal relationships that could have appeared to influence the work reported in this paper.

☐The authors declare the following financial interests/personal relationships which may be considered as potential competing interests:

HIGHLIGHTS

- SfM was used to obtain a high-resolution topography of an urban drainage model
- Overland flow of few millimeters from 3 rainfalls were measured by means of LSPIV
- Fluorescent particles were used as LSPIV tracers to avoid raindrops interference
- 2D shallow water model was used to assed SfM and LSPIV experimental data